Research article

Halloysite nanotubes as delivery mechanism for feather protein-based multi-surfactant systems in crude oil dispersion application

Yaw Kwakye Adofo , Emmanuel Nyankson [*], Benjamin Agyei-Tuffour , Selassie Gbogbo , Christian Amoako , Joseph Arko Morgan , Gloria Pokuaa Manu , Grace Karikari Arkorful

Material Science and Engineering Department, School of Engineering Sciences, University of Ghana, Legon-Accra, Ghana

A B S T R A C T

Chicken feather protein (CFP), and lecithin (L), Tween 80 (T), and DOSS (D) surfactant systems were loaded onto halloysite nanotubes (HNTs), a natural clay aluminosilicate product to form particulate dispersants at different surfactant concentrations and characterized by Fourier Transform Infrared spectroscopy, thermogravimetric analysis and scanning electron microscopy coupled with EDS. For 24 wt% surfactants concentrations loaded HNTs; 100 wt%CFP-HNTs, 60 wt%CFP- 40 wt%L-HNTs, 20 wt%CFP- 80 wt%T-HNTs, 50 wt%CFP- 25 wt%T-25 wt%L-HNTs and 25 wt %CFP- 25 wt%T-50 wt%D-HNTs showed good interfacial tension lowering abilities by recording 6.39, 2.82, 2.43, 1.68, and 1.55 mN/m at 60s respectively. The CFP-based surfactant-HNTs dispersants formed very stable o/w emulsions against droplet coalescence and showed an increase in interfacial viscosity which contributed to the stability of their respective o/w emulsions. In this study, the US EPA's baffled flask test was deployed to probe the prospects of the CFP-based surfactants-HNTs dispersants in crude oil dispersion at different surfactant concentrations. 100 wt%CFP-HNTs, 60 wt %CFP- 40 wt %L-HNTs, 20 wt %CFP- 80 wt %T-HNTs, 50 wt %CFP- 25 wt%T-25 wt%L-HNTs and 25 wt%CFP- 25 wt%T-50 wt%D-HNTs recorded dispersion effectiveness of 33.9, 74.8, 65.4, 78.6 and 88.2 vol% respectively at 24 wt% surfactant concentration. It can be deduced that an increase in the surfactant concentrations loaded onto HNTs improved the dispersion effectiveness of the produced particulate dispersants. Largely, the 24 wt% CFP-based surfactant-HNTs dispersants showed considerable promise in crude oil dispersion in seawater.

1. Introduction

Applying chemical dispersants is a well-known emergency cleanup strategy popularly deployed during the largest oil spill incident in April 2010 [1,2]. It is generally applied to oil slicks on the surface of the water to expedite the breaking up of the surface oil into minute droplet sizes in the presence of mechanical energy for onward microbial depletion in the water column [3,4]. The composition of commercially available dispersants is more often than not two or more surfactants mixed in a solvent and are culturally liquid [1,5].

For so many years and much more recently, solid particles have continuously been investigated for their ability to adsorb at the oil-

water (o/w) interface and are being utilized in many fields like catalysis, drug delivery, synthesis of materials, water treatment, emulsion stabilization in cosmetic and food science applications and crude oil spill dispersion [6–8].

When solid particles that tend to adsorb at the o/w interface are used to create an emulsion, the emulsion is referred to as Pickering emulsion [9,10]. Using solid particles to stabilize emulsions as well as its potential effectiveness in crude oil spill remediation has drawn broader interest because of its numerous merits over regular liquid dispersants. Solid particles have an edge over liquid dispersants because they can form stable o/w emulsions at lower concentrations [11]. Emulsions formed from solid particles in general are more stable to oil droplet coalescence than that of amphiphilic surfactant stabilized emulsions [12]. Using solid particles in oil spill dispersion gives a higher chance of visible feedback to spill response teams [13]. Solid particle dispersants will most likely ensure a higher dispersant-to-oil contact rate due to a relatively long buoyancy period as well as an increase in viscosity of emulsions by forming a 3D viscous linkage in water and this could promote the formation of stable emulsions [13,14]. Logistically, it is easier to deal with solid particles in terms of storage and transport [4,6].

Several studies have been conducted on Pickering emulsions using different types of solid particles in the process. These particles include montmorillonite, bentonite clay, silica, carbon black, iron oxide, graphene oxide, polystyrene, and halloysite clay nanotubes (HNTs/HNT) [15,16].

Dong et al. [14] reported on an eco-friendly montmorillonite clay particle functionalized with bis (2-hydroxyethyl) oleylamine surfactant. They reported that dodecane/artificial seawater emulsions that were created had good stability against droplet coalescence and to a large extent, a surfactant concentration of 0.001 % w/v was able to facilitate stable dodecane/seawater emulsion formation. They further asserted that stable emulsions and smaller droplet sizes were obtained because of an increase in the viscosity of the aqueous phase and a reduction in electrostatic repulsion between the adsorbed clay particles.

While chemical surfactants stabilize emulsions by lowering the interfacial tension of the o/w interface, solid particle-stabilized emulsions occur using the particles assembling at the o/w interface to provide steric blocks against droplet coalescence [10]. Many factors such as morphology, size of particles (micro/nanometers), chemical nature of particles, etc. may affect the stability of Pickering emulsions but one major influencing factor in the formation of Pickering emulsions is the wettability of particles [6,10]. For Pickering emulsions to form, solid particles must be partially wetted by both oil and water phases because this forces particle partitioning towards the o/w interface [6,17]. Particle-formed emulsions are known to be highly stable and the reason behind this phenomenon is that the energy that can necessitate the desorption of a particle from the o/w interface into either the dispersed or continuous phase is huge [18]. For example, for HNTs which are cylindrical in morphology, when used in o/w emulsion stabilization, the energy required to desorb a particle from the o/w interface can be expressed mathematically as;

$$\Delta E_{des} = 2RL \; \gamma_{o/w} \; [\sin(\theta) - \theta\cos(\theta) \; [1 + R/L] + R\cos^2(\theta)\sin(\theta)L] \tag{1}$$

In which ΔE_{des} = Desorption energy, R = Cross-sectional radius, L = Cylindrical particle length, $\gamma_{o/w}$ = Interfacial tension of o/w interface, and θ = Wetting contact angle [17].

Assuming a particle of radius = 50 nm, length = 1.5 μm, $\gamma_{o/w}$ = 50 mN/m and θ = 29° (knowing that the 3-phase contact angle of HNTs/water/oil is < 30° [6]) and inserting into equation (1) gives 8.74×10^4 kT. Therefore, the energy required to remove a particle from the o/w interface spontaneously is extremely high and this makes it almost impossible.

HNTs per se have reportedly been used for various applications such as emulsion stabilization as well as nano-vehicles to deliver drugs and bio/chemically active ingredients for crude oil spill cleanup.

Yu et al. [11] in their study concluded that polypeptoid functionalized HNTs adequately lowered o/w interfacial tension, improved the thermodynamic tendency of the solid particles to partition at the o/w interface, and exhibited an increase in the viscosity of emulsions which provided resistance to the coalescence of droplets.

Wei et al. [19] investigated the use of HNTs as an improved mechanism to deliver antiseptics more efficiently. In this study, brilliant green, iodine, and amoxicillin were loaded onto HNTs and examined respectively. They were able to show in their study that HNTs can be used to slowly release antiseptics with enhanced anti-microbial actions for prolonged durations.

Nyankson et al. [20] conducted a study to use surfactant-loaded HNTs as dispersants for crude oil spill dispersion. In the study, they reported that HNTs were altered with Lecithin FPI, Span 80, and Tween 80. They concluded that ternary surfactants loaded onto HNTs recorded dispersion effectiveness of 99 vol% in a baffled flask test.

HNTs in their natural form are hydrated solid inorganic materials made up of aluminosilicate sheets in the form of rolls [21]. They are expressed stoichiometrically as $Al_2Si_2O_5[OH]_4.nH_2O$ where n could be either 2 or 0 and represent the two forms of HNTs [6,22]. When n = 2, then HNTs are hydrated and referred to as halloysite-10 Å which possess a single layer of water molecules between its multilayers [21,23]. When n = 0, the resulting version is the dehydrated halloysite-7Å which occurs by a phase transition with loss of adsorbed water as HNTs are heated within the range of 60-150°C [23,24]. HNTs are a tubule structure with a hollow lumen, non-toxic, biocompatible, and readily available in the environment [20]. The walls of HNTs are made up of 15–20 rolled layers of Al_2O_3 and SiO_2 with an aspect spacing of 0.72 nm [21,23]. Generally, HNTs on the market possess an external diameter averaging between 50 and 200 nm [6]. They also possess an inner lumen diameter averaging between 15 and 50 nm and a tubular length within the range of 0.5–2 μm [6,21]. HNTs possess a distinct surface chemistry in which the external surface is composed of silica and the internal surface is made of alumina [25]. Given this, the external and internal surfaces of HNTs possess opposite charges in water of pH ranging from 2 to 8 [24,26]. This is a result of differing ionization and dielectric properties of Al_2O_3 (positively charged) and SiO_2 (negatively charged) [21,26]. Nonetheless, the general electrical zeta potential of HNTs is taken as almost that of the zeta potential of silica which forms the outer composition [21,25]. HNTs possess various unique characteristics that make them suitable for this study and they include large surface area, high aspect ratio, high thermal and mechanical stability, adaptable aspect chemistry, and a distinct tube-like morphology

[11,27]. The high aspect ratio and tube-like particle morphology cause an increase in the energy needed for a particle to desorb from the o/w interface spontaneously [11]. The distinct tube-like morphology promotes stuffing of the internal lumen with various chemical and bioactive ingredients such as surfactants and protein macromolecules, thereby serving as a medium of delivery [23,28,29]. Although the external surface and the interstitial spaces between adjacent HNTs can be considered as carrier means, the lumen can be considered as the primary delivery mechanism of HNTs [30]. Using HNTs in such applications is important because it promotes the safe and effective delivery of these chemicals/bioactive ingredients to the intended target.

HNTs are highly hydrophilic materials that do not promote effective o/w emulsion stabilization when used alone [11,17]. So, to improve upon the ability of HNTs to stabilize emulsions, the surfaces are often modified to regulate the hydrophilic-lipophilic balance (HLB) to a point suitable for stable emulsion formation [10,20]. The external surface chemistry of HNTs allows surface modification because of the presence of appropriate functional groups such as silanol [11]. As inferred by Nyankson et al. [20], surfactants can be used to alter the HLB of HNTs and the surfactant-solid particle couple stands a higher chance of forming very stable o/w emulsions. Until the introduction of surfactants, the HNTs' wetting ability influences an attachment to the aqueous phase [31]. When surfactants are loaded onto HNTs, the particle wettability is altered towards the oil phase, thus the surfactant-solid particles become partially wetted by both the oil and aqueous phase and this gives room for enhanced emulsion stability [10,17,31].

When surfactants are coupled with HNTs, they can achieve ideal stabilization because, in the presence of mixed energy, the surfactants adsorb at the o/w interface to provide stability by lowering the interfacial tension whereas the particles ensure the stability of emulsions by assembling at the o/w interface to provide steric blocks, electrostatic repulsion(where particles are charged and provide repulsive interactions between oil droplets) and increase in interfacial viscosity which provides resistance against the thinning of interceding liquid when droplets come closer to each other and this prevents droplets from coalescing [15,32,33]. HNTs have a parallel alignment to the o/w interface and this ensures a broader contact area where the steric blocks inhibit fluctuations that can promote the coalescence of oil droplets [34]. HNTs facilitate good dispersion by attaching firmly onto the o/w interface, then stabilizing the interface, and finally releasing the surfactants which provide the interfacial tension-lowering effect and this leads to the formation of discrete oil droplets [17,20,35].

In situations whereby the lumen of HNTs is stuffed with surfactants purposefully for oil dispersion, it can be said that traditional amphiphilic emulsions have been coupled with Pickering emulsions to form particulate dispersants and the synergistic interaction has the propensity to enhance crude oil dispersion [12,20,34].

In this study, chicken feather protein (CFP) reported by Adofo et al. [36] to be a good natural emulsifier and a prospect in crude oil spill remediation was coupled with HNTs. CFP-based binary and ternary dispersants formulated by combining CFP, Lecithin(L), Tween 80(T), and Dioctyl Sodium Sulfosuccinate Salt (DOSS) also referred to as D in some parts of the study were also coupled with HNTs respectively.

This work is a continuous study on Adofo et al. [36] and the goal is to blend CFP with other surfactants and combine with HNTs to formulate particulate dispersants to enhance the dispersion effectiveness of the CFP while eliminating the usual toxic petroleum-based solvents used in traditional dispersant formulations. The specific objectives to realizing our goal are (i) using HNTs as delivery vessels for the respective CFP-surfactant systems to increase the dispersant-oil contact rate while minimizing the amount of dispersant that comes in contact with the aqueous phase (ii) replacing organic solvents with solid particles, eco-friendly HNTs which can influence stable emulsion formation as well as to reduce the chemical content of formulated dispersants.

This study covers CFP, Lecithin, Tween 80, and DOSS surfactant systems loaded onto HNTs respectively. The emulsions formulated from the respective particulate dispersant systems were observed and discussed. The effect of viscosity on emulsion stability was also investigated. The dynamic interfacial tension of the particulate dispersant systems was examined and discussed respectively. The dispersion effectiveness of the respective particulate dispersant systems was probed using the baffled flask test procedure.

2. Experimental section

2.1. Materials

Protein extract from chicken feathers. Every chemical employed in this study was of analytical grade and was utilized without additional purification. Halloysite clay nanotubes, Soy Lecithin, Tween 80, and Dioctyl Sodium Sulfosuccinate Salt (DOSS), were purchased from Sigma Aldrich. Ethanol and Dichloromethane (DCM) were bought from VWR Chemicals. The Instant Ocean Salt was purchased from Spectrum Brands Pet LLC (Blacksburg, VA), and Deionized water. The light crude oil was collected from the OCTP Sankofa oil field in Ghana (The crude oil characteristics were determined as; kinematic viscosity = 4.658 cSt measured @ 40 °C, API gravity of 35.04° and density = 849.3 kg/m^3).

2.2. Method

2.2.1. Chicken feather protein characterization

The chicken feather protein extract was characterized by FT-IR and NMR analysis respectively as reported by Adofo et al. [36].

2.2.2. Synthetic (artificial) seawater preparation

Synthetic seawater of 35 ppt was prepared by dissolving 35g of the instant ocean salt in one (1) liter of deionized water and mixed in a volumetric flask. The resulting solution was placed on a Cole-Parmer StableTemp stirrer at 250 rpm for 24 h to guarantee the particles were wholly dissolved. The pH of the synthetic seawater was measured to be 7.8 using the benchtop pH meter and was done in

triplicate.

2.2.3. CFP-based surfactants loading onto HNTs

The procedure adopted for this study was similar to that reported by Nyankson et al. [17] and Owoseni et al. [37]. 2g mass of 100 wt%CFP surfactant was measured into a beaker. 45 ml of ethanol was added to the beaker. 5 ml of deionized water was added to the beaker to make a 100 wt%CFP surfactant solution of 40 mg/ml. The solution was stirred for 5 min on a Cole-Parmer StableTemp stirrer. A 2g mass of raw HNT was weighed into a beaker. 6 ml of the 100 wt%CFP surfactant solution was measured and added to HNT in the beaker to form a slurry. The mixture was placed in a vacuum jar and vacuum suction was applied for 5 min and the pressure was let go after the period. The vacuum suction procedure was repeated seven times. The sample was dried in an oven at 60 °C for 12 h. They were collected in the form of dry 100 wt%CFP-HNTs particles. The total concentration in weight percentage for 100 wt%CFP loaded onto HNTs was 12 wt%. This procedure was repeated for the binary and ternary CFP-based surfactant systems of respective surfactant ratios (20 wt%CFP-80 wt%Tween 80,60 wt%CFP-40 wt%L, 50 wt%CFP-25 wt%T-25 wt%L and 25 wt%CFP-25 wt%T-50 wt%D) to obtain 12 wt% of respective surfactant systems loaded onto HNTs. The same procedure was repeated for loading 24 wt% of all CFP-based surfactant systems onto HNTs except for the volume of surfactant solution, for which 12 ml was used, the vacuum suction, which was performed fourteen times, and the resulting samples were dried in an oven at 60 °C for 30 h. All samples were collected as dry particles.

2.2.4. Characterization of CFP-based surfactants-HNTs particulate dispersants and raw HNTs

CFP-based surfactants-HNT particles and raw HNTs were characterized by Fourier Transform Infrared (FT-IR) analysis, Thermogravimetric analysis (TGA), and Scanning electron microscopy (SEM) coupled with EDS.

2.2.4.1. TGA analysis.
TGA of 24 wt% CFP-based surfactants-HNTs respectively and raw HNTs were performed using the Q600 SDT ta instrument (Troemner, waters – LLC). The analyses were conducted over a temperature range of 0–800 °C with a heating rate of 10 °C/min and nitrogen gas was used as the purge gas. The sample weight analyzed was between 1 and 10 mg. The TA Universal Analyzer software was used to further analyze the data obtained during the cycle of heating.

2.2.4.2. FT-IR analysis.
The Bruker Platinum-ATR FT-IR spectrometer (S/N 104605) with infrared spectra 400-4000 cm^{-1} was employed for the analyses. The OPUS 7.5 software connected to the equipment was used to analyze the results. The mass of each sample analyzed was approximately 3 mg.

2.2.4.3. SEM images of CFP-based Surfactants-HNTs and raw HNT.
The morphology of the 24 wt% CFP-based surfactant systems loaded on HNTs respectively and raw HNTs were examined using the MIRA3 TESCAN scanning electron microscopy coupled with EDS acquiring detector. The basic components of the CFP-surfactants-HNTs systems and HNTs were investigated via EDS. The beam energy and working distance used were 5.0 kV and 4.69–5.43 mm respectively.

2.2.5. Emulsion stability and viscosity tests

2.2.5.1. Emulsion stability test.
200 mg of raw HNTs was added to 10 ml of synthetic seawater in a glass vial and vortexed at 2000 rpm for 1 min 1 ml of crude oil was added to the mixture and vortexed for 2.5 min at 2500 rpm on the Stuart vortex mixer (CAT no. SA8). After removing the mechanical energy, the emulsion was allowed to rest for one (1) hour and monitored. Photographs of the o/w emulsion were taken after the resting period to discuss the stability of the emulsions created. This method was repeated for all 24 wt% CFP-based surfactants-HNTs respectively. The experiment was done in duplicates respectively. To further understand the observations made in this study, optical microscopy and droplet size distribution of respective emulsions formed were examined.

2.2.5.2. Optical microscopic view of emulsions and droplet size determination.
Optical micrographs were taken of the o/w emulsions produced by mixing 200 mg of CFP-based surfactants-HNTs and raw HNTs respectively with 1 ml of crude oil, and 10 ml of synthetic seawater. The ensuing mixtures were vortexed at 2500 rpm for 2.5 min on the Stuart vortex mixer (CAT no. SA8). After a settling period of one (1) hour, a small aliquot of the respective o/w emulsions was collected on a glass slide and covered with a cover slip for optical microscopy. The micrographs were taken using AmScope FMA050.

2.2.5.3. Viscosity of formulated emulsions.
A measured mass of raw HNTs and each of the 24 wt% CFP-based surfactant-HNTs were used to prepare o/w emulsions respectively. Using a 1 ml of crude oil to 10 ml of synthetic seawater, the respective solid particles were added and vortexed at 2500 rpm for 2.5 min respectively. The dynamic viscosities of each of the CFP-based surfactants-HNTs and raw HNTs

respectively as well as that of crude oil-synthetic seawater emulsions were measured at a temperature of 28 °C respectively utilizing the Cole-Parmer viscometer (SN: VCPR140021). The viscosity for each formulated emulsion was measured two times and the average viscosity was worked out.

2.2.6. Dynamic interfacial tension activity of particulate dispersants

Applying the Du Noüy ring method, the dynamic interfacial tension of the synthetic seawater, CFP-based surfactants-HNTs, raw
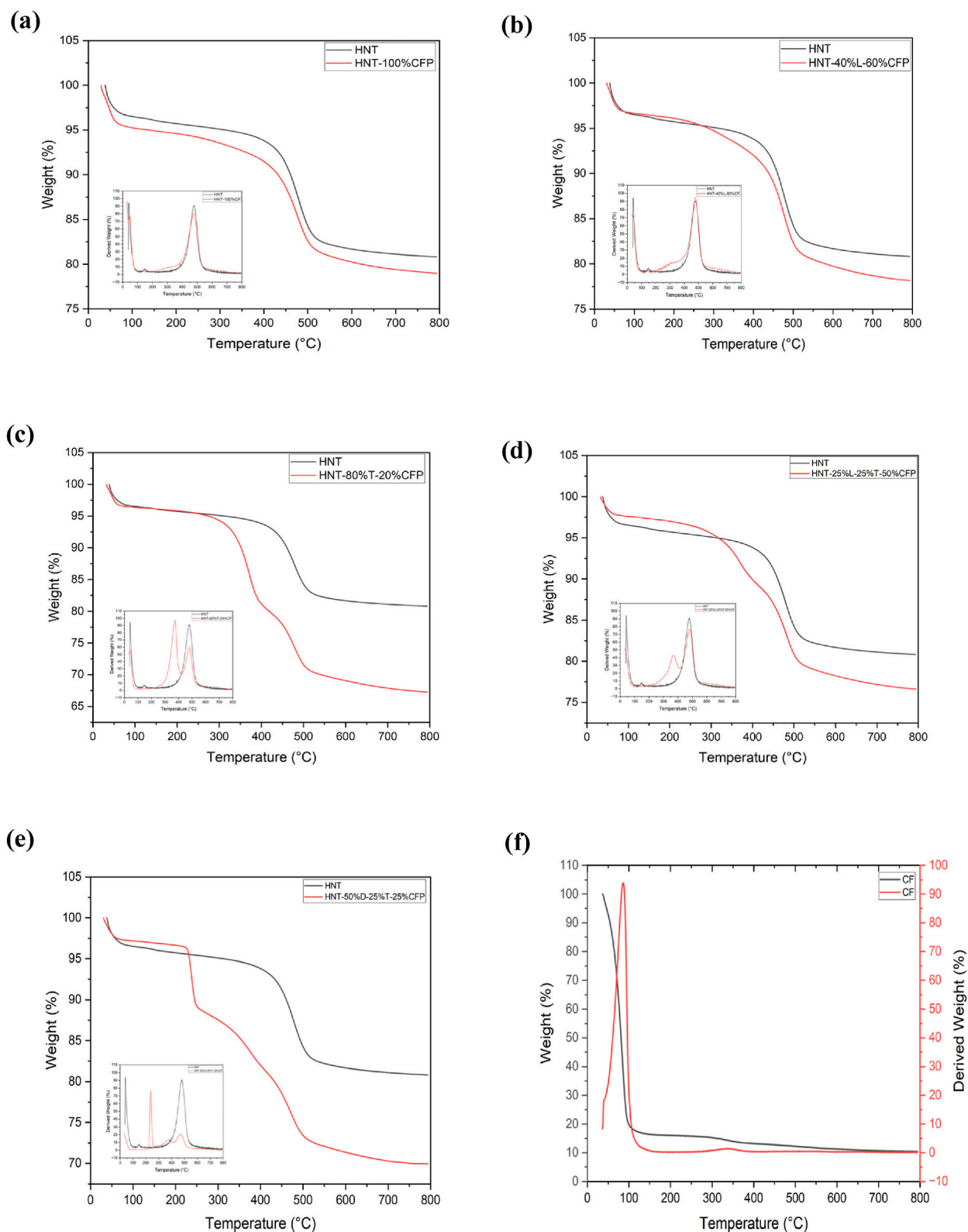
Fig. 1. 24 wt% CFP-based surfactants loaded onto HNTs (a–e) (a) 100 wt%CFP-HNTs (b) 60 wt%CFP-40 wt%L-HNTs (c) 80 wt%CFP-20 wt%T-HNTs (d) 50%wt.CFP-25 wt%T- 25 wt%L-HNTs (e) 25 wt%CFP-25 wt%T- 50 wt%D-HNTs. (f) TGA analysis of 100 wt%CFP.

HNTs, and the crude oil systems were analyzed respectively using the Biolin Scientific digital tensiometer (Sigma701, SN 71168).

Synthetic seawater-crude oil dynamic interfacial tension was measured at 28 °C by measuring synthetic seawater into a glass cuvette to about two-thirds full. The probe was hanged and dipped into the synthetic seawater. 5 ml of crude oil was dispensed gently onto the top of the synthetic seawater. The probe was lifted closer to the interface but remained in the aqueous phase and the instrument was started. Using the OneAttension software, the dynamic interfacial tension value was calculated. The method was repeated for the addition of the CFP-based surfactants-HNTs and raw HNTs respectively to the synthetic seawater-crude oil. The mass of solid particles used in conducting the test was 10 mg respectively. Test for each sample was conducted in triplicate.

2.2.7. Dispersion effectiveness of particulate dispersants

An effectiveness examination was conducted to ascertain the ability of the formulated particulate dispersants to disperse the Sankofa crude oil in seawater. The dispersion effectiveness (DE) of the raw HNTs and all the 12 wt% CFP-based surfactant-HNTs dispersants were probed respectively through the US EPA's baffled flask test [33]. An almost identical approach to Venosa et al.'s [38] baffled flask test (BFT) protocol was employed in this probe. Measuring 120 ml of synthetic seawater in the baffled flask (250 mL), an amount of Crude oil (100 μl) was attentively dispensed directly onto the top of the synthetic seawater in the baffled flask utilizing a 10–100 μl Pipet4u micropipette. 500 mg of the raw HNTs and each of the 12 wt% CFP-based surfactant-HNT dispersants were introduced into a baffled flask for the respective examination. It was conducted attentively so that the dispersant does not first touch the synthetic seawater but the oil. Each baffled flask was agitated for a 10-min duration at 200 rpm on an advanced digital shaker (VWR 3500). After the 10 min period of agitation, the flask remained gentle for another 10 min. After the 10-min calm period, a small quantity (2 ml) of each of the baffled flask contents was discharged from the stop cork and thrown away. A quantity of 30 ml of each o/w emulsion formed was collected into 100 ml graduated cylinders respectively. Each of the 30 ml samples held in a graduated cylinder was transferred into a separation funnel (250 ml) and each was extracted twice using 10 ml fresh DCM, making the whole measure of DCM 20 ml per sample. The dispersed oil contained in each extracted sample was evaluated using UV–vis spectroscopy at an absorbance wavelength range of 300–400 nm. The BFT procedure was repeated for all the 24 wt% CFP-based surfactant-HNTs dispersants formulated in their respective proportions. All experiments in this study were conducted at room temperature and performed three times.

3. Results and discussion

3.1. CFP characterization

FT-IR spectroscopy and Nuclear Magnetic Resonance analysis were used to characterize the CFP extract as detailed in Adofo et al. [36], a study that was conducted to determine the prospect of CFP in crude oil dispersion. They showed that CFP contains amino acids and is a remarkable source of protein.

3.2. Characterization of CFP-based surfactants-HNTs products

3.2.1. Thermal stability of particulate dispersants

The vacuum suction approach was used to load respective CFP-based surfactant systems onto the HNTs. To examine the thermal properties of the respective surfactants loaded HNTs, the evaluation was done using TGA. TGA was adapted to observe the weight change the respective samples experienced in the presence of temperature as shown in Fig. 1 for 24 wt% CFP-based surfactants loaded onto HNTs.

In Fig. 1(a), there were two clear decompositions observed in the raw HNTs sample at about 41 °C and 480 °C. There was mass loss at 41 °C due to the decomposition of water molecules adsorbed onto the HNTs surface and the mass loss seen at 480 °C could be pinned on dihydroxylation of the HNTs. There were two clear decompositions observed in the CFP surfactant-loaded HNT sample at about 48 °C and 480 °C. There was a mass loss at 48 °C due to the decomposition of water molecules from the liquid protein extract and the mass loss at 480 °C was because of dihydroxylation of HNTs.

In Fig. 1(b), there were three clear decompositions observed in the CFP-L surfactant-loaded HNT sample at about 41 °C, 242 °C, and 480 °C. There was a mass loss at 41 °C due to the decomposition of water molecules from the liquid CFP extract. The mass loss that was recorded at about 242 °C can be directed at the thermal degradation of the lecithin and the mass loss seen at 480 °C because of dihydroxylation of HNTs.

In Fig. 1(c), there were three clear decompositions observed in the CFP-T surfactant-loaded HNT sample at about 42 °C, 375 °C, and 482 °C. There was a mass loss at 42 °C due to the decomposition of water molecules from the liquid CFP extract. The mass loss that was recorded at about 375 °C can be directed at the thermal degradation of the Tween 80 surfactant and the mass loss at 482 °C because of dihydroxylation of HNTs.

In Fig. 1(d), there were four clear decompositions observed in the CFP-T-L surfactant-loaded HNT sample at about 41 °C, 216 °C, 371 °C, and 484 °C. There was a mass loss at 41 °C due to the
decomposition of water molecules from the liquid CFP extract. The mass loss that was recorded at about 216 °C can be directed at the thermal degradation of Lecithin and that which was recorded at about 371 °C can be pinned on the thermal degradation of the Tween 80 surfactant. The mass loss at 484 °C can be a result of dihydroxylation of HNTs.

In Fig. 1(e), there were four clear decompositions observed in the CFP-T-D surfactant-loaded HNT sample at about 41 °C, 237 °C, 369 °C and 480 °C. There was a mass loss at 41 °C due to the decomposition of water molecules from the liquid CFP extract. The mass

loss recorded at about 237 °C can be directed at the thermal degradation of DOSS and that which was recorded at about 369 °C can be directed at the thermal degradation of the Tween 80. The mass loss at 480 °C can be a result of the dihydroxylation of HNTs.

The thermal degradations which occurred at temperature ranges of 216 °C–375 °C point out that the CFP-based surfactants were loaded onto the HNTs. The decomposition of the CFP looks like that of the raw HNT in Fig. 1(a) because, the CFP used was in liquid form and after the decomposition of the water from the protein graph, it was observed that the protein showed total stability as shown in Fig. 1(f).

At the end of the thermal stability studies, it was found that (as shown in Fig. 1) the various particulate dispersant formulations exhibited a degree of thermal stability respectively after decomposition.

3.2.2. FT-IR analyses of particulate dispersants

Further investigations using FT-1R analyses were conducted for the CFP-based surfactants loaded HNTs and raw HNTs to identify functional groups present in the respective specimen. This investigation was conducted for the 24 wt% CFP-based surfactants loaded onto HNTs in which six major peaks (seen for all specimens) plus two other peaks (seen for all specimens except raw HNTs) as presented in Fig. 2 were observed and discussed in Table 1 below.

The two Additional peaks which were observed for the CFP-based surfactants loaded-HNTs occurred at 2845 cm⁻1 and 2965 cm⁻1 respectively and further confirmed that these CFP-based surfactants were truly loaded onto the HNTs [17].

3.2.3. Scanning electron microscopy and component identification of particulate dispersants

As shown in Fig. 3(a), the SEM image of raw HNTs proved their known cylindrical morphology. As shown in Fig. 3(c–e, g, i and k), the 24 wt% CFP-based surfactants loaded-HNTs showed an agglomeration which could mean that some of the surfactants occupied the interstitial spaces between neighboring HNTs. The general sticky nature of the loaded surfactants, lecithin, DOSS, Tween 80 (moderately viscous), and CFP (moderately viscous) also contributed to the clustering of the particles as seen in their respective images.

In Fig. 3 (b) the elemental components of raw HNTs can be seen as C, O, Al, and Si. The presence of Al and Si confirms that the particles analyzed were truly HNTs ($Al_2Si_2O_5[OH]_4 \cdot nH_2O$). It can be seen from the EDS spectrum that Al and Si have a molar ratio of approximately 1:1. In Fig. 3 (d) the elemental components of 100 wt%CFP-HNTs can be seen as C, O, Na, Al, and Si. The Al and Si presence indicates the availability of HNTs while the C and O represent the carbonyl presence in the CFP sample. The small amount of Na seen could be a result of CFP being purified with Sodium hydroxide solution during the extraction process as reported by Adofo et al. [36]. In Fig. 3 (f) the elemental components of 60 wt%CFP-40 wt%L- HNTs can be seen as C, O, Al, and Si. The Al and Si presence indicates the availability of HNTs while the C and O indicate that CFP and lecithin are present since carbon and oxygen form the basis of protein and lecithin. In Fig. 3 (h) the elemental components of 20 wt%CFP-80 wt%T- HNTs can be seen as C, O, Al, and Si. The Al and Si presence indicates the availability of HNTs while the C and O indicate that CFP and Tween 80 are present since carbon and oxygen form the basis of protein and Tween 80. In Fig. 3 (j) the elemental components of 50 wt%CFP- 25 wt%T-25 wt%L-HNTs can be seen as C, O, Al, and Si. The Al and Si presence indicates the availability of HNTs while the C and O indicate that CFP, Tween 80, and lecithin
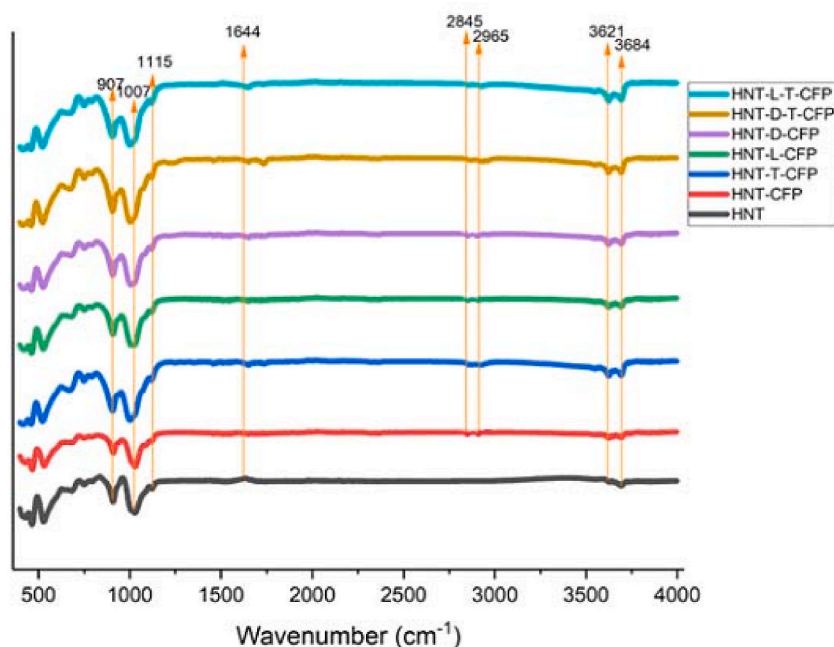

Fig. 2. The FT-IR graph representing 24 wt% CFP-based surfactants-HNTs and raw HNT.

Table 1

Peak observations of FT-IR spectra analysis for CFP-based surfactants-HNTs and raw HNTs.

Peaks (cm^{-1})	Explanation
3684	This can be seen due to the stretching vibrations of the inner-surface hydroxyl groups [14,17]
3621	Also seen because of the stretching vibrations of inner-surface hydroxyl groups [14,17]
2965	Peak occurred due to the symmetric and asymmetric stretching of CH$_2$ [14,17].
2845	This peak was seen because of the symmetric and asymmetric stretching of CH$_2$ [17,32].
1644	Occurred because of the deformational vibration of the interlayer water [14,32]
1115	Caused by the stretching mode of epical Si–O [17,32]
1007	This peak occurred because of the stretching vibrations of Si–O–Si [14,17]
907	This peak occurred because of the deformation vibration of the inner surface hydroxyl groups of the HNTs [17,32]
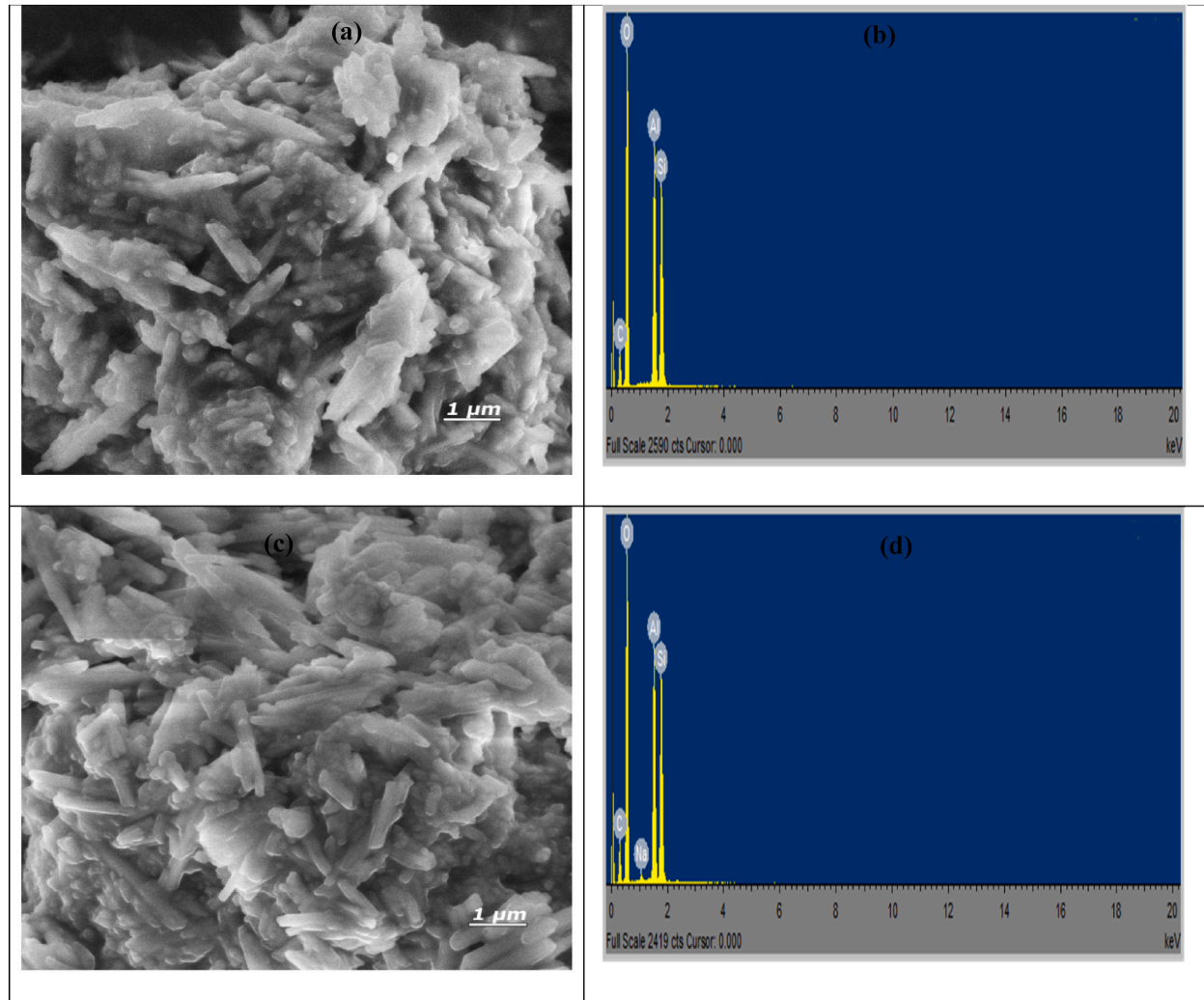
Fig. 3. (a) SEM images of raw HNTs (b) EDS spectra of raw HNTs (c) SEM images of 100 wt%CFP- HNTs (d) EDS spectra of 100 wt%CFP- HNTs (e) SEM images of 60 wt%CFP- 40 wt%L-HNTs (f) EDS spectra of 60 wt%CFP- 40 wt%L-HNTs (g) SEM images of 20 wt%CFP- 80 wt%T-HNTs (h) EDS spectra of 20 wt%CFP- 80 wt%T-HNTs (i) SEM images of 50 wt%CFP- 25 wt%T-25 wt%L-HNTs (j) EDS spectra of 50 wt%CFP- 25 wt%T-25 wt%L-HNTs (k) SEM images of 25 wt%CFP- 25 wt%T-50 wt%D-HNTs (l) EDS spectra of 25 wt%CFP- 25 wt%T-50 wt%D-HNTs.

are present since carbon and oxygen form the basis of protein, Tween 80 and lecithin.

In Fig. 3 (l) the elemental components of 25 wt%CFP- 25 wt%T-50 wt%D-HNTs can be seen as C, O, Na, Al, Si, and S. The Al and Si presence indicates the availability of HNTs while the C and O indicate that CFP and Tween 80 are present. The availability of Na and S confirms the presence of DOSS in the specimen.
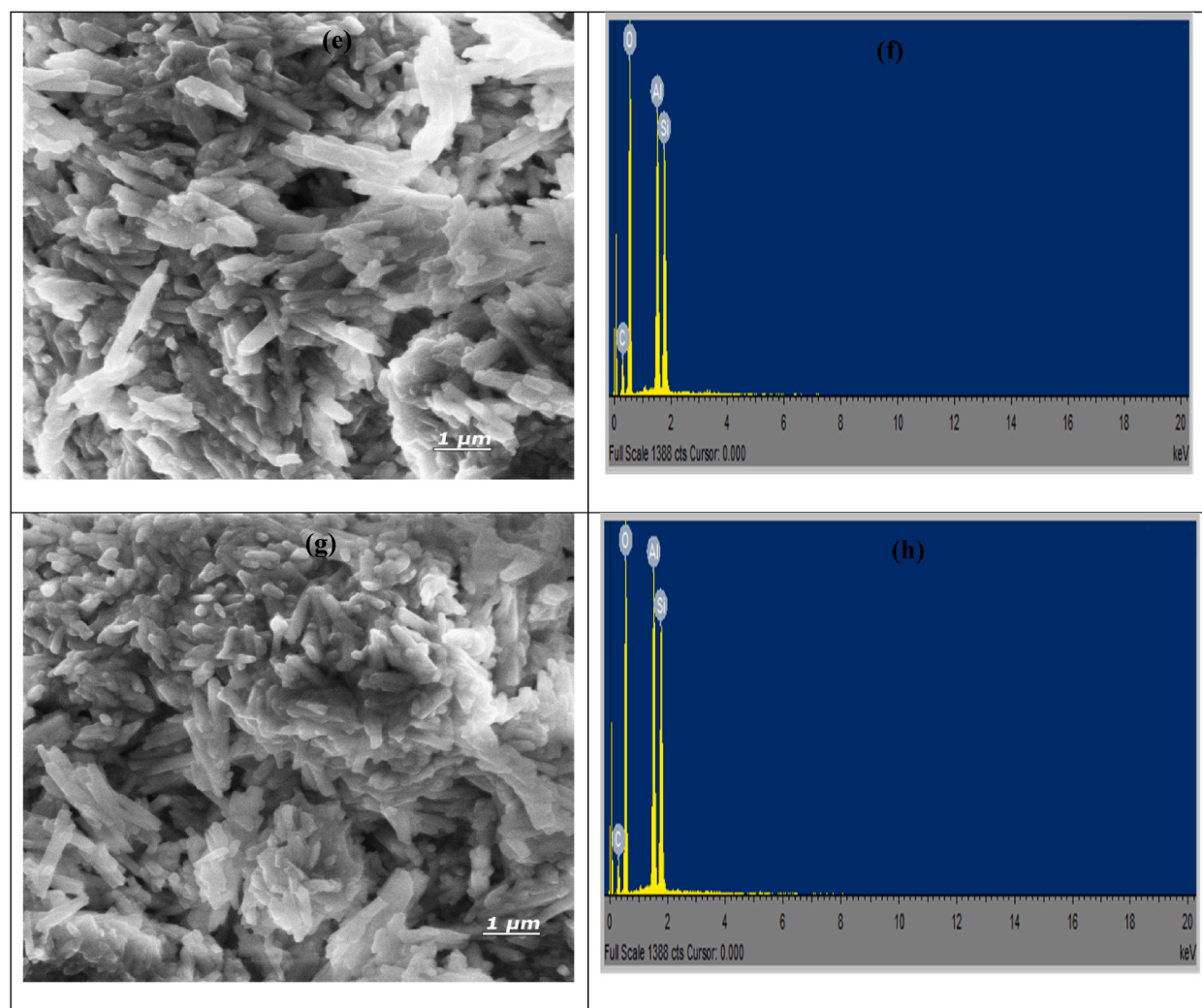
Fig. 3. (*continued*).

3.3. Studies on emulsion formation and stability for particulate dispersants

Solid particle-formed dispersants have been reported to have the ability to generate stable o/w emulsions [20,39]. In this study, raw HNTs and the respective 24 wt% CFP-based surfactants loaded onto HNTs were used to form o/w emulsions, monitored for 1 h, and discussed. Images of respective o/w emulsions after 1 h are presented in Fig. 4.

Fig. 4(a) shows o/w emulsion formed by raw HNTs. After the given period, creaming had rapidly occurred and almost a complete phase separation can be seen. This means that o/w emulsions formed with raw HNTs had destabilized after an hour. This observation can be attributed to the fact that raw HNTs are reportedly known to be highly hydrophilic substances (particle wettability leans towards the aqueous phase) and do not effectively form stable o/w emulsions when not functionalized [8]. It can also be seen from Fig. 4 (b–f) that the CFP-based surfactants-HNTs o/w emulsions formed showed high turbidity and slow creaming rate at an hour period which implies that they remained stable. When solid particles (e.g. HNTs) are functionalized with surface active ingredients to alter their wettability to an appropriate balance which supports effective o/w emulsion formation, they can combine synergistically at the o/w interface as shown in Fig. 5 to form very stable emulsions [37,40]. In this case, HNTs provide stability by forming steric blocks against drop coalescence at the o/w interface while the surfactants adsorb at the interface and lower the interfacial tension to enhance emulsion stability [10,40,41].

In Fig. 4(b) the CFP which is a good natural emulsifier interacted synergistically with the HNTs to form a stable o/w emulsion. In Fig. 4(c) CFP and lecithin at a ratio of 60-40 % interact synergistically as surfactants because lecithin can form water-in-oil microstructures and this aids in solubilizing CFP in the oil phase thus promoting interfacial tension reduction. Also, a synergistic interaction occurred between these two surfactants and HNTs at the o/w interface [42]. This led to a close packing assembly at the o/w interface to reduce interfacial tension significantly. Hence, combining 60 wt%CFP-40 wt%L and HNTs results in an enhanced o/w emulsion
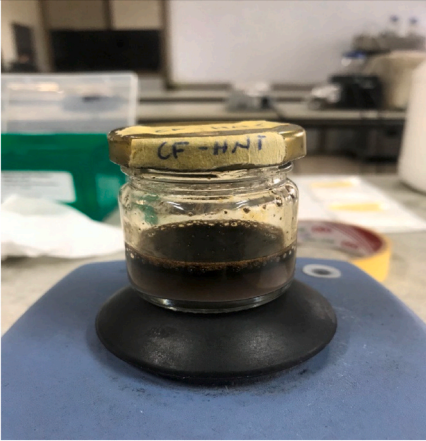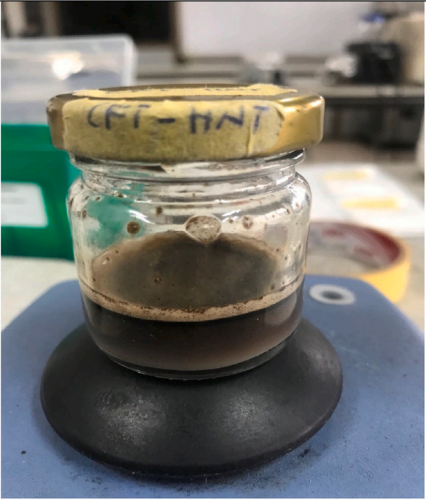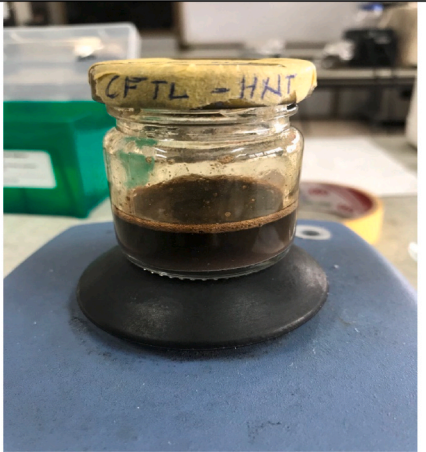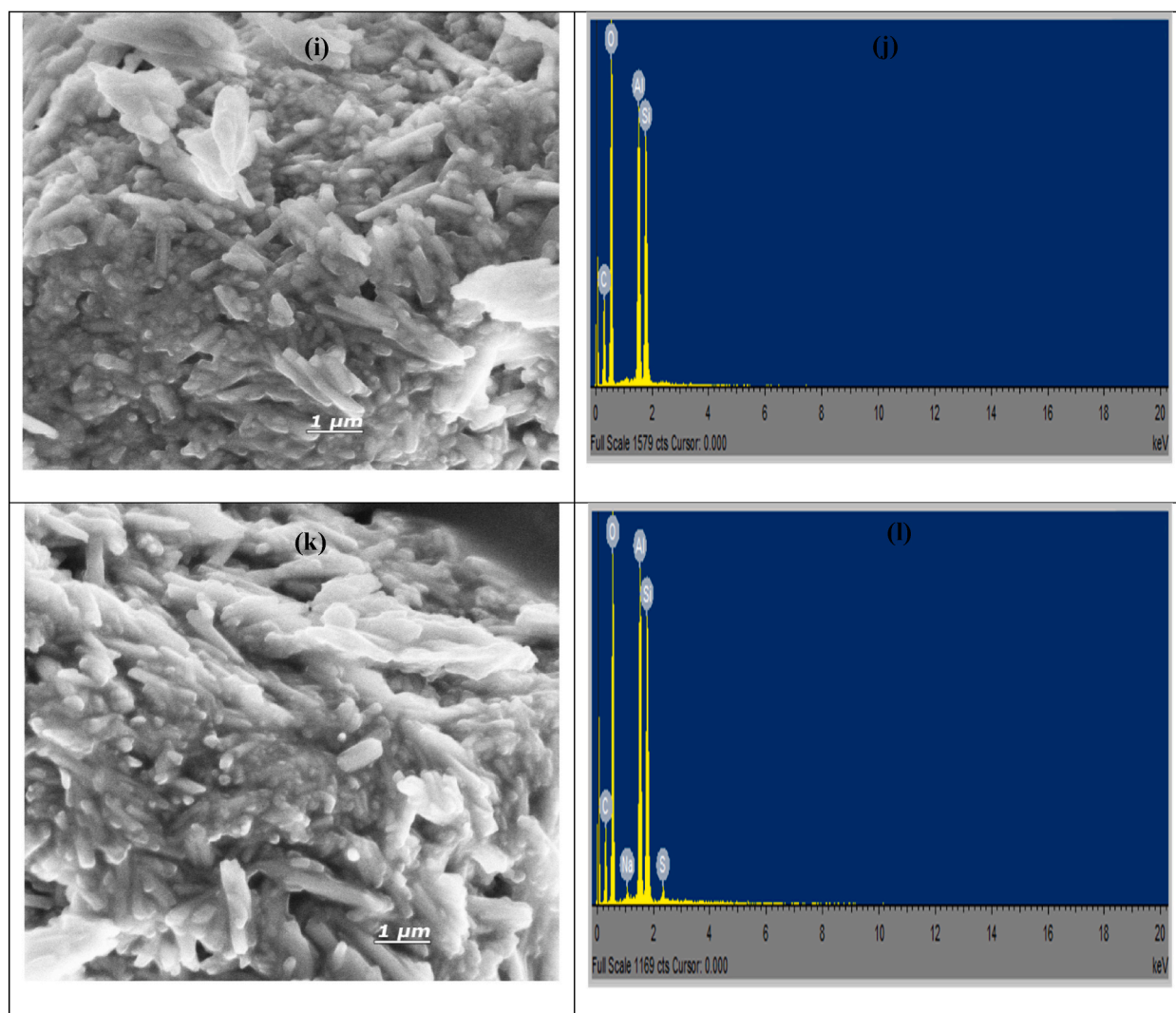
Fig. 3. (*continued*).

stability. In Fig. 4(d), CFP-T at a ratio of 20-80 wt% interact synergistically because when proteins and Tween 80 are combined, they likely result in chaperoning properties at the o/w interface which promotes significant interfacial tension reduction [43]. Hence, combining 20 wt%CFP-80 wt%T and HNTs resulted in a synergistic interaction between the surfactants and particles which led to enhanced o/w emulsion stability [44]. In Fig. 4(e) CFP-Tween 80-Lecithin at the ratio of 50-25-25 wt% interact synergistically because lecithin can form water-in-oil microstructures and this aids in solubilizing CFP and Tween 80 in the oil phase which promotes significant interfacial tension reduction [42,43]. Hence, combining 50 wt%CFP-25 wt%T-25 wt%L and HNTs results in an enhanced o/w emulsion stability. In Fig. 4(f), CFP-Tween 80-DOSS at the ratio of 25-25-50 wt% interact synergistically because DOSS can form water-in-oil microstructures and this aids in solubilizing CFP and Tween 80 in the oil phase [37,38]. This leads to a close packing assembly at the o/w interface to reduce interfacial tension significantly. Hence, combining 25 wt%CFP-25 wt%T-50 wt%D and HNTs leads to another synergistic interaction between surfactants and particles which resulted in an enhanced o/w emulsion stability. Observations made under this study were further confirmed by optical microscopic studies and droplet size distribution as shown in Fig. 6.

3.4. Optical micrographs and droplet size distribution of particulate dispersants

Micrographs of o/w emulsions produced with raw HNTs and the 24 wt% CFP-based surfactants-HNTs respectively, synthetic seawater and Sankofa crude oil, and their droplet size distribution were evaluated by randomly picking 280 emulsion droplets after 1-h duration given for settling are presented in Fig. 6. The rationale behind this study is to further understand the observations made in Fig. 4.

(a) Raw HNTs	(b) 100wt.%CFP-HNT

(c) 60wt.%CFP-40wt.%L-HNT	(d) 20wt.%CFP-80wt.%T-HNT

(e) 50wt.%CFP-25wt.%T-25wt.%L-HNT	(f) 25wt.%CFP-25wt.%T-50wt.%D-HNT

(caption on next page)

Fig. 4. Crude oil/synthetic seawater emulsions formed by (a) raw HNTs (b) 100 wt%CFP-HNTs (c) 60 wt%CFP-40 wt%L-HNTs (d) 20w.t%CFP-80 wt%T-HNTs (e) 50 wt%CFP-25 wt%T-25 wt%L-HNTs (f) 25 wt%CFP-2wt.5%T-50 wt%D-HNTs.

In Fig. 6(a) the solid particles as well as interfacial film could not provide enough resistance against emulsion destabilization over the given period. Creaming had fast occurred, and few droplets remained in the water phase. Fig. 6(b) represents the average droplet size of emulsions formed by the raw HNT which was computed to be 72.3 μm. For Fig. 6(c, e, g, i, and k), the solid particles are attached to the surfaces of oil droplets. This creates steric hindrance against droplet coalescence as well as causes a likely increase in interfacial viscosity which may contribute to the stability of the respective emulsions whilst the presence of respective CFP-based surfactants at the o/w interface promotes interfacial tension reduction leading to the formation of tiny droplets. Fig. 6(d–f, h, j and l) represents the average droplet sizes of emulsions formed by 100 wt%CFP- HNTs, 60 wt%CFP- 40 wt%L-HNTs, 20 wt%CFP- 80 wt%T-HNTs, 50 wt% CFP- 25 wt%T-25 wt%L-HNTs and 25 wt%CFP- 25 wt%T-50 wt%D-HNTs respectively and the values obtained are 36.2, 42.9, 33.8, 35.6 and 34.2 μm respectively.

Results obtained in this study confirm the observations made in Fig. 4.

3.5. Impact of viscosity on emulsion stability

Dynamic viscosity measurements were taken for crude oil-seawater, the raw HNTs o/w emulsion, and all the 24 wt% CFP-based surfactant-HNTs emulsions at a temperature of 28 °C respectively. Records of the respective average viscosities for the o/w emulsions are presented in Table 2.

From the table, dynamic viscosity recorded for raw HNTs o/w emulsions and that of crude oil-synthetic seawater formed did not have any significant difference. This means that raw HNTs could not attach firmly to the droplets to increase viscosity, and this influenced the destabilization of raw HNTs formulated o/w emulsions in this case [8,14]. This confirms the observation made in Fig. 4 (a). Comparing the viscosities recorded for the CFP-based surfactants-HNTs respectively to that of crude oil-synthetic seawater without dispersant, there was a significant increase in the viscosities of emulsions formed by the CFP-based surfactants-HNTs respectively. This could be a result of CFP-based surfactants-HNT particles firmly attaching to droplets at the o/w interface [8].

As stated earlier, it is known that an increase in interfacial viscosity provides resistance against the thinning of intervening liquid when droplets come closer to each other and this prevents droplets from coalescing [9,11,28]. This promotes the formation of discrete droplets as well as enhances the stability of o/w emulsions. This further confirms the observations made in Fig. 4(b–f). Hence, it can be
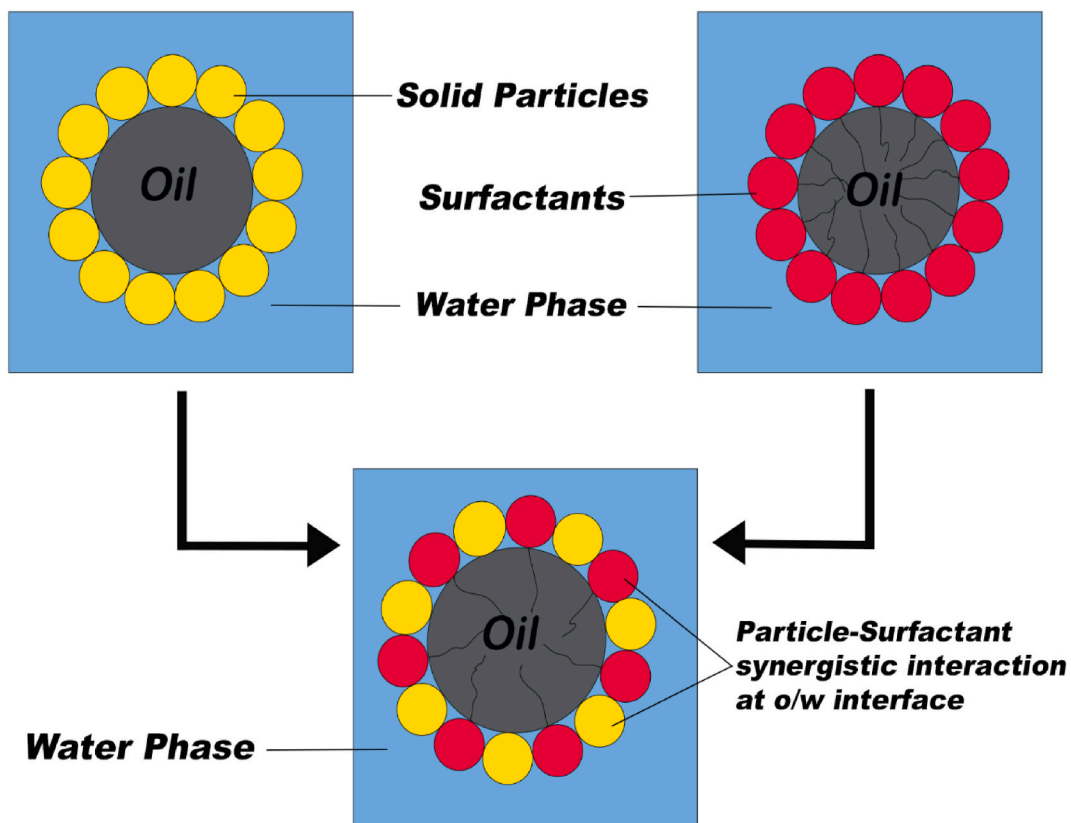
Fig. 5. Synergistic interaction between components of particulate dispersant at the o/w interface.
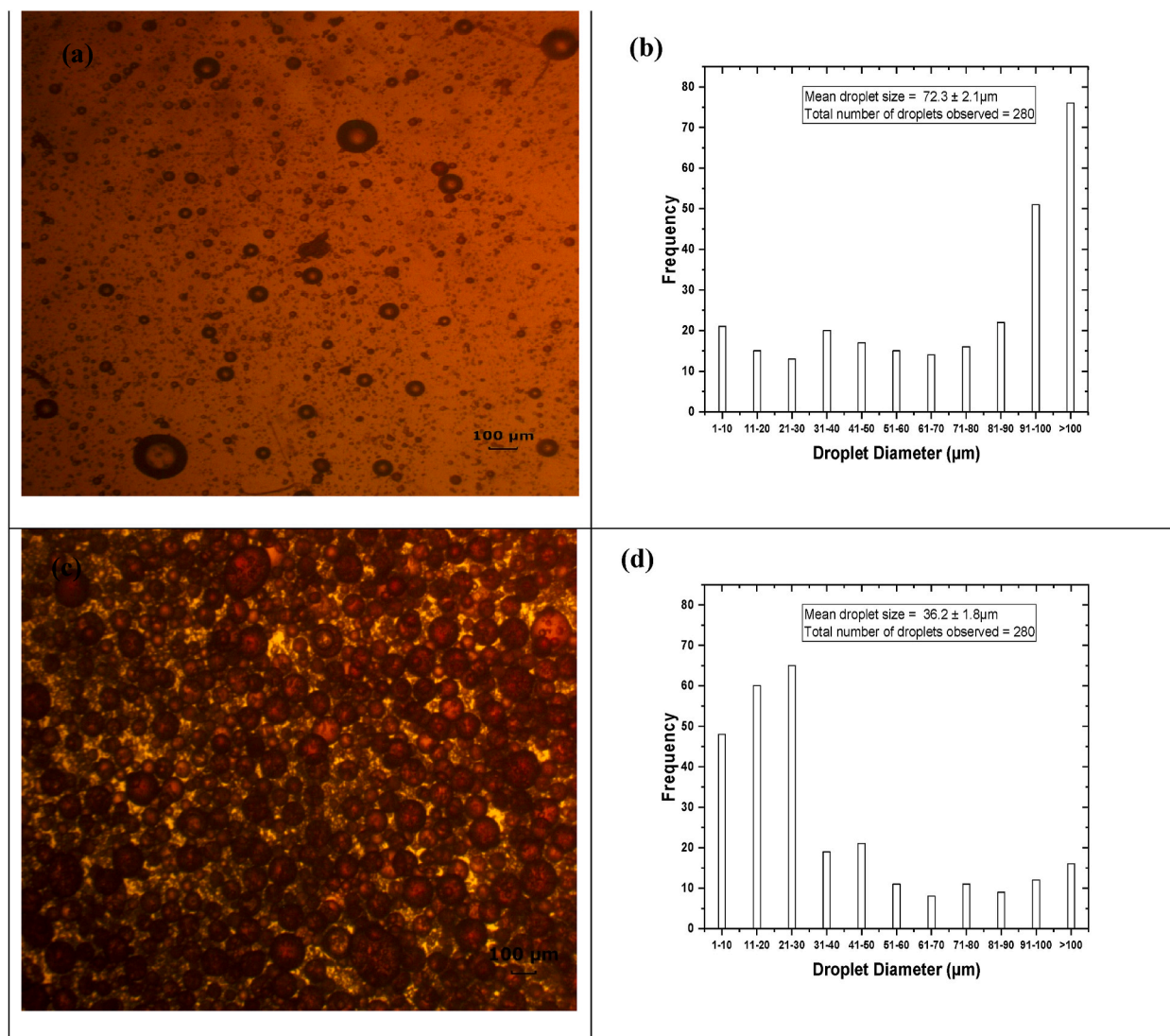
Fig. 6. (a) Micrograph of raw HNTs (b) droplet sizes of raw HNTs (c) micrograph of 100 wt%CFP- HNTs (d) droplet sizes of 100 wt%CFP- HNTs (e) micrograph of 60 wt%CFP- 40 wt%L-HNTs (f) droplet sizes of 60 wt%CFP- 40 wt%L-HNTs (g) micrograph of 20%CFP- 80%T-HNTs (h) droplet sizes of 20%CFP- 80%T-HNTs (i) micrograph of 50%CFP- 25%T-25%L-HNTs (j) droplet sizes of 50 wt%CFP- 25 wt%T-25 wt%L-HNTs (k) micrograph of 25 wt%CFP- 25 wt%T-50 wt%D-HNTs (l) droplet sizes of 25 wt%CFP- 25 wt%T-50 wt%D-HNTs.

said that an increase in interfacial viscosity influences o/w emulsion stability.

3.6. Interfacial activity of particulate dispersants

The dynamic interfacial tension at the air-synthetic seawater interface was first measured and recorded as 71.8 mN/m at 28 °C. At the same 28 °C, the interfacial tension at the Sankofa crude oil-synthetic seawater interface was subsequently measured to be 17.9 mN/m. Both recordings were made in 60s.

The dynamic interfacial tension was measured for Raw HNTs, 100 wt%CFP- HNTs, 60 wt%CFP- 40 wt%L-HNTs, 20 wt%CFP- 80 wt%T-HNTs, 50 wt%CFP- 25 wt%T-25 wt%L-HNTs and 25 wt%CFP- 25 wt%T-50 wt%D-HNTs for 12 wt% and 24 wt% CFP-based surfactants loaded onto HNTs respectively.

As shown in Fig. 7, Raw HNTs, 100 wt%CFP- HNTs, 60 wt%CFP- 40 wt%L-HNTs, 20 wt%CFP- 80 wt%T-HNTs, 50 wt%CFP- 25 wt%T-25 wt%L-HNTs and 25 wt%CFP- 25 wt%T-50 wt%D-HNTs recorded 16.4, 6.39, 2.82, 2.43, 1.68, 1.55 mN/m at 60s period respectively.

Raw HNTs did not cause much change in the interfacial tension at the crude oil-synthetic seawater interface. This is because raw
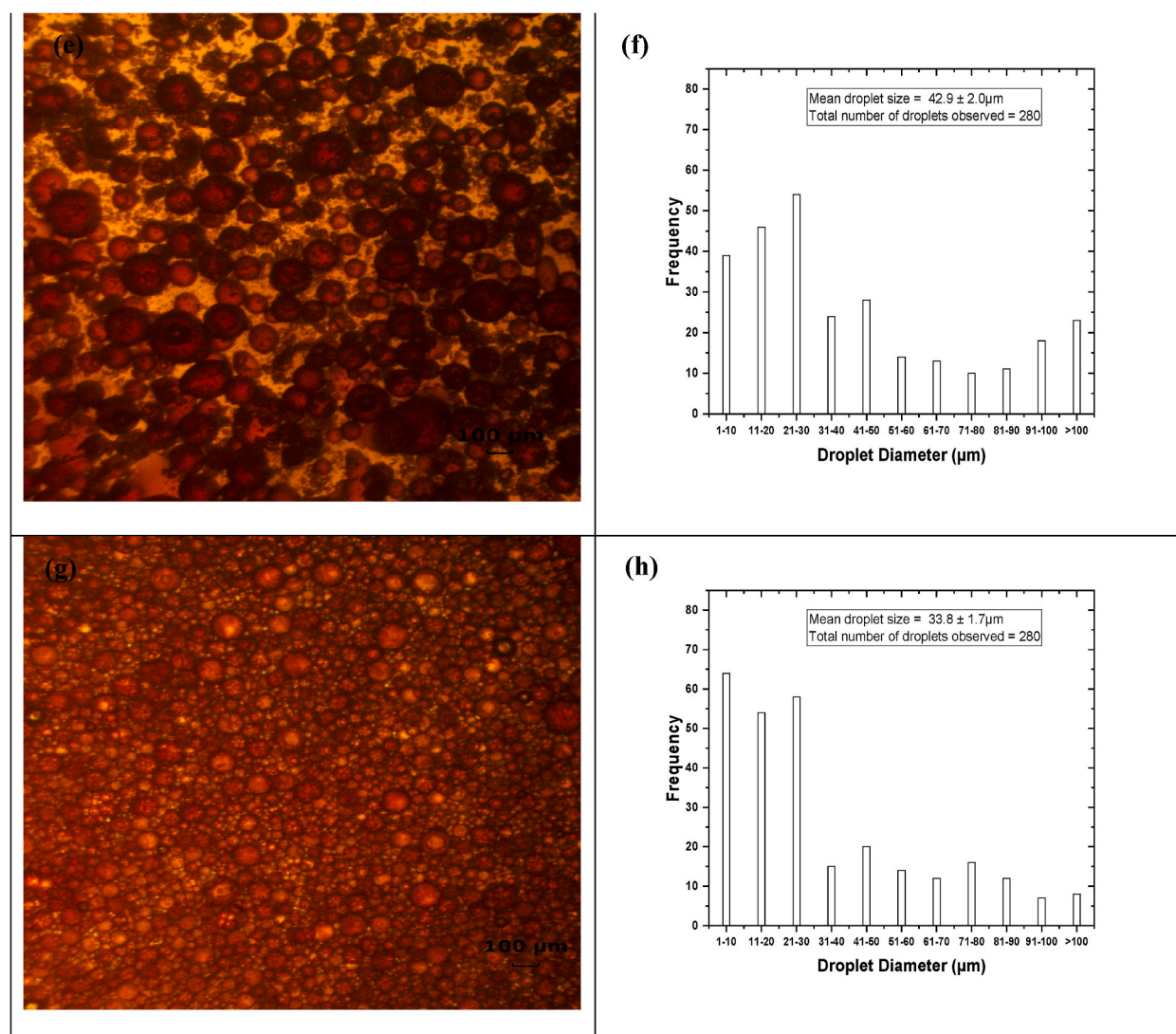
Fig. 6. (*continued*).

HNTs are highly hydrophilic to effectively adsorb at the o/w interface without surface modification and do not possess interfacial tension reduction properties, therefore are not good for lowering interfacial tension [14,32]. All the CFP-based surfactants-HNTs dispersants significantly lowered the o/w interfacial tension respectively. This is because the HNTs have been enhanced with surface active ingredients which can adsorb at the o/w interface when released from their HNT containers. When this occurs, the surfactants being amphiphiles naturally, align at the o/w interface to cause a drastic decrease in the o/w interfacial tension.

Ward et al. [30] reported that the loading of surfactants onto HNTs can occur in three areas and they are, getting attached to the internal and/or external of the HNTs through electrostatic forces, inhabiting the interstitial spaces between neighboring HNTs as crystallites and they inhabiting the lumen of the HNTs. Although this study does not delve into the release kinetics of the CFP-based surfactants from the HNTs, it can be seen from Fig. 7 that a drastic decrease in interfacial tension was recorded at 60s followed by a gradual decrease in interfacial tensions recorded at the subsequent times respectively. This occurrence can be a result of the burst release of CFP-based surfactants from the interstitial spaces between neighboring HNTs at the o/w interface [22,45]. The gradual reduction in interfacial tension that followed the initial drastic reduction could be a result of CFP-based surfactants gently releasing from the lumen of the HNTs as well as from the surface and/or inner walls of HNTs [22,45].

3.7. Dispersion effectiveness of particulate dispersants

In this study, the prospect of raw HNTs, 100 wt%CFP- HNTs, 60 wt%CFP- 40 wt%L-HNTs, 20 wt%CFP- 80 wt%T-HNTs, 50 wt% CFP- 25 wt%T-25 wt%L-HNTs and 25 wt%CFP- 25 wt%T-50 wt%D-HNTs to disperse crude oil in seawater were explored using BFT.
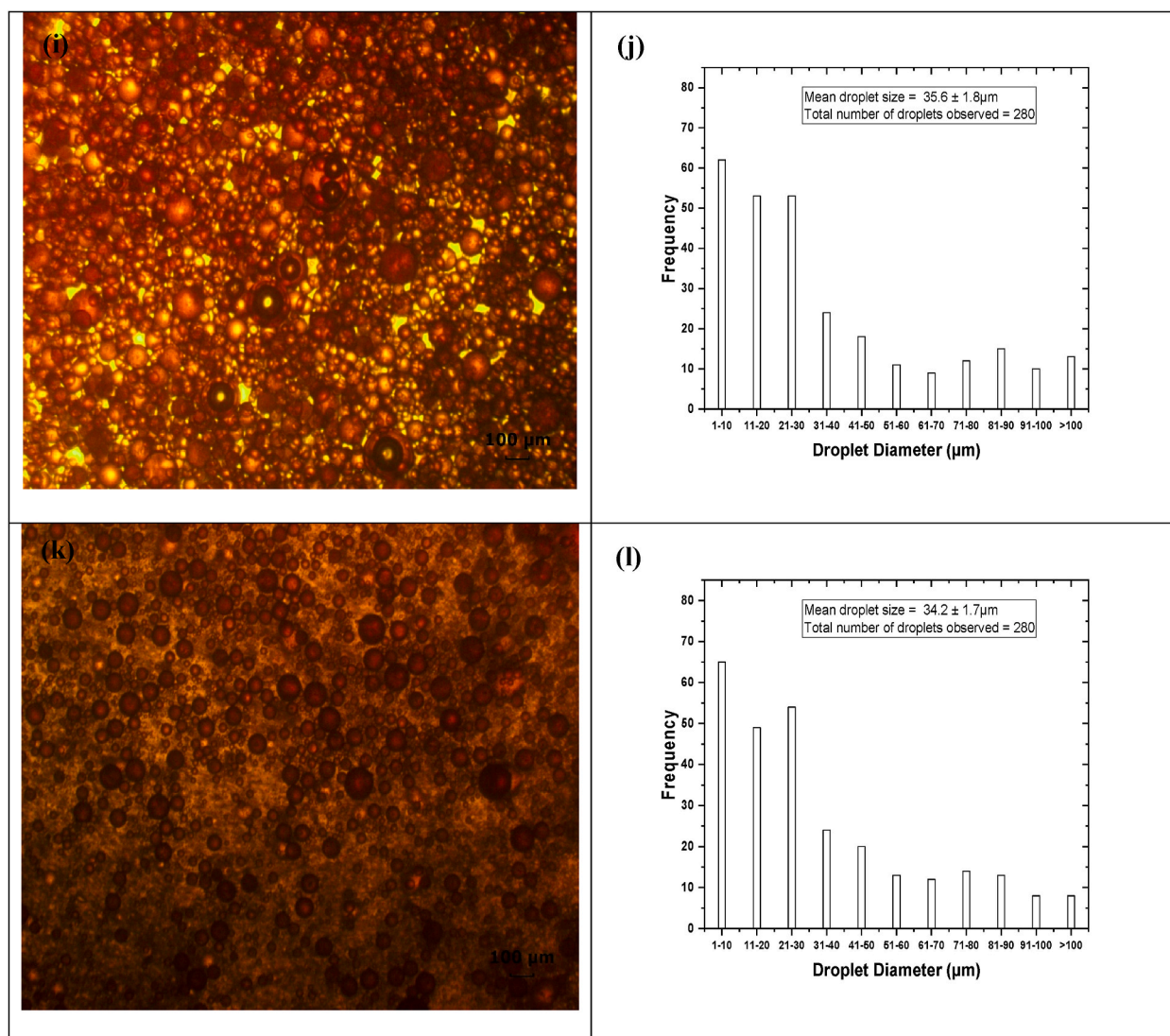
Fig. 6. (*continued*).

Table 2
Dynamic viscosity measurements of o/w emulsions formulated using particulate dispersants.

O/W Emulsion Contents	Viscosity (MPa.s)
Crude oil + synthetic seawater (no dispersant added)	14.6
Raw HNTs + Crude oil + synthetic seawater	14.9
100%CFP-HNTs + Crude oil + synthetic seawater	17.1
60%CFP-40%L-HNTs + Crude oil + synthetic seawater	17.6
20%CFP-80%T-HNTs + Crude oil + synthetic seawater	17.7
50%CFP-25%T-25%L-HNTs + Crude oil + synthetic seawater	18.0
25%CFP-25%T-50%D-HNTs + Crude oil + synthetic seawater	17.5

Two different concentrations (24 wt% and 12 wt%) of CFP-based surfactant systems loaded onto HNTs were considered as shown in Fig. 8.

From Fig. 8, raw HNTs recorded a dispersion effectiveness of approximately 5 vol%. This value was the least recorded value for all the particulate dispersants examined. This is because raw HNTs are very hydrophilic with their particle wettability inclined towards the water phase and this does not support the effective formation of stable o/w emulsions [8,14]. They do not possess interfacial tension reduction characteristics and cannot effectively aid in the break-up of oil into minute droplets. For 100 wt%CFP- HNTs, 60 wt% CFP- 40 wt%L-HNTs, 20 wt%CFP- 80 wt%T-HNTs, 50 wt%CFP- 25 wt%T-25 wt%L-HNTs and 25 wt%CFP- 25 wt%T-50 wt%D-HNTs,
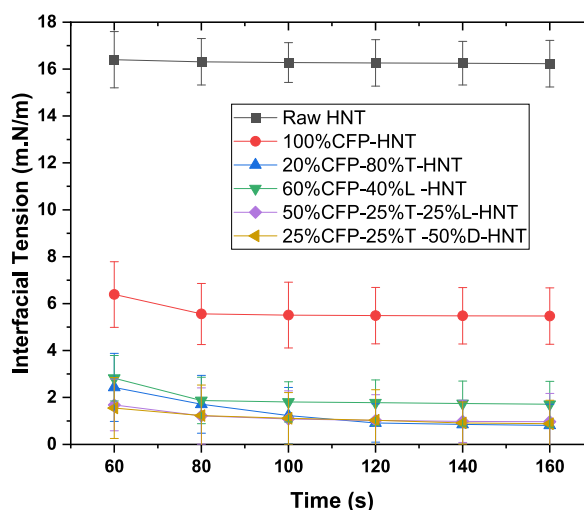
Fig. 7. Interfacial tension of raw HNTs and 24 wt% CFP-based surfactants-HNTs dispersants.
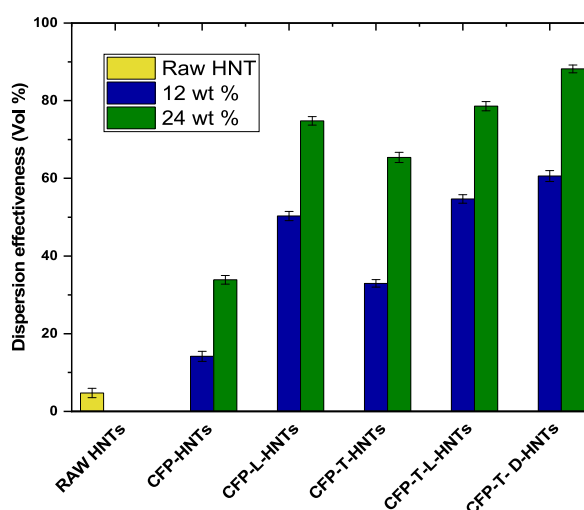

Fig. 8. Dispersion effectiveness of CFP-based surfactants-HNTs dispersants.

they recorded dispersion effectiveness of 33.9, 74.8, 65.4, 78.6 and 88.2 vol% respectively at 24 wt% CFP-based surfactants loaded onto HNTs. At 12 wt% CFP-based surfactants loaded onto HNTs, they recorded a dispersion effectiveness of 14.2, 50.3, 33.0, 54.7, and 60.6 respectively. Comparing the dispersion effectiveness of raw HNTs to that of the CFP-based surfactants loaded onto HNTs, it can be deduced that altering the surface of HNTs with the surfactants led to a change in the surface chemistry of the HNTs leading to an improved dispersion effectiveness [8]. While the HNT particles hold firmly onto the oil at the o/w interface to resist droplet coalescence, they release the surfactants for subsequent lowering of interfacial tension and oil breaks up into minute drops in the presence of mixed energy [8,27]. The synergy between the CFP-based surfactants and HNTs led to improved dispersion effectiveness.

Looking at the dispersion effectiveness values recorded by the 12 wt% CFP-based surfactants-HNTs dispersants compared to the of the 24 wt% CFP-based surfactants-HNTs, it can be said that the concentration of dispersants influences the effectiveness of dispersion. Generally, the 24 wt% particulate dispersants performed better than the 12 wt% particulate dispersants and it could be because at increased concentrations, more surfactants became available for adsorption at the o/w interface which led to a more effective interfacial tension reduction as reported earlier. This phenomenon can be said to have led to the better dispersion effectiveness performance recorded by the 24 wt% CFP-based surfactants-HNTs dispersants.

Considering the research conducted by Nyankson et al. [20], the surface of HNTs was modified by Tween 80, lecithin PI, and DOSS surfactants respectively. After investigating the dispersion effectiveness of the respective particulate dispersant formulations using the US EPAs baffled flask test, HNT-Tween 80, HNT-Lecithin PI, and HNT-DOSS recorded dispersion effectiveness of 69.1, 62.8, and 44.9 vol% respectively. Although testing conditions may vary, comparatively, it can largely be seen that the dispersion effectiveness obtained from the 24 wt% particulate dispersants in this study show a greater potential for crude oil remediation in seawater and this

could be a result of combining multiple surfactants onto the HNTs [17,37].

4. Conclusion

This study aimed at enhancing the potential of the CFP in crude oil dispersion as reported by Adofo et al. [36] as well as minimize the chemical components of the formulated dispersants by eliminating the use of regular petroleum-based solvents. By using halloysite nanotubes as a means to deliver CFP-based multi-surfactant systems onto crude oil in seawater, the primary rationale was to increase the dispersant-oil contact rate and reduce the aqueous solubility of the formulated dispersants, to enhance their potential in crude oil dispersion. Secondly, was to eliminate the use of organic solvents [46]. These were achieved by successfully loading 100 wt%CFP, 60 wt%CFP- 40 wt%L, 20 wt%CFP-80 wt%T, 50 wt%CFP- 25 wt%T-25 wt%L and 25 wt%CFP- 25 wt%T-50 wt%D at different concentrations onto HNTs and examining them respectively. The 24 wt% CFP-based surfactants-HNTs dispersants used for the emulsion stability studies formed very stable o/w emulsions compared to that of the raw HNTs. The results indicate that HNTs coupled with the CFP-based surfactants aid in breaking up oil slicks into minute droplet sizes which can grant a large surface area for onward microbial consumption in the seawater column leading to an effective oil dispersion [10,47]. It was shown in this study that interfacial viscosity promotes the formation of stable emulsions since the respective o/w emulsions formed from the particulate dispersants remained stable over the given period.

It can be concluded that raw HNTs are poor at lowering interfacial tension while CFP-based surfactants-HNTs dispersants reduced significantly the interfacial tensions at the o/w interface respectively.

In terms of dispersion effectiveness, a minimum of 45 vol% in a standard laboratory test can necessitate a dispersant formulation to be listed on the US EPAs National Contingency Plan (NCP) product schedule [48], given this, raw HNTs were very poor at dispersing crude oil in seawater whiles the 100 wt%CFP-HNTs can also be said to be ineffective considering the 33.0 vol% dispersion effectiveness recorded at 24 wt%. This figure obtained is not far away from the target and could be improved in subsequent studies. All the 24 wt% binary and ternary CFP-based surfactants-HNTs showed great potential and demonstrated to be effective at crude oil dispersion. It can further be deduced from this study that, an increase in surfactant concentration caused an increase in dispersion effectiveness of the particulate dispersants.

In conclusion, CFP-based surfactants loaded onto HNTs at 24 wt% interacted synergistically and formed stable o/w emulsions, increased the interfacial viscosity of o/w emulsions formed, reduced o/w interfacial tension remarkably, and facilitated the break-up of oil into minute droplets. They largely exhibited improved crude oil spill dispersion effectiveness in seawater when compared to that of the liquid CFP dispersant alone as reported by Adofo et al. [36]. This indicates that the CFP-based particulate dispersants have a good potential in crude oil dispersion application.

CRediT authorship contribution statement

Yaw Kwakye Adofo: Writing – original draft, Resources, Methodology, Investigation, Formal analysis, Conceptualization. **Emmanuel Nyankson:** Validation, Supervision, Resources, Methodology, Conceptualization. **Benjamin Agyei-Tuffour:** Validation, Supervision, Resources. **Selassie Gbogbo:** Investigation. **Christian Amoako:** Writing – review & editing, Investigation. **Joseph Arko Morgan:** Writing – original draft, Investigation. **Gloria Pokuaa Manu:** Validation, Investigation. **Grace Karikari Arkorful:** Investigation.

Disclosure statement

The authors declare no competing interest.

Data availability statement

In this research work, no data was used.

Declaration of competing interest

The authors declare that they have no known competing financial interests or personal relationships that could have appeared to influence the work reported in this paper.

Acknowledgment

References

[1] Y.K. Adofo, E. Nyankson, B. Agyei-Tuffour, Dispersants as an oil spill clean-up technique in the marine environment: a review, Heliyon 8 (8) (2022) e10153.

[2] Z. Cai, et al., Effects of oil dispersants on settling of marine sediment particles and particle-facilitated distribution and transport of oil components, Mar. Pollut. Bull. 114 (1) (2017) 408–418.

[3] W. Li, et al., Effects of oil properties on the formation of oil-particle aggregates at the presence of chemical dispersant in baffled flask tests, J. Hazard Mater. 436 (2022) 129227.

[4] S. Gbogbo, et al., Multicomponent Photocatalytic-dispersant system for oil spill remediation, ACS Omega 9 (8) (2024) 8797–8809.

[5] Q. Cai, et al., A cross-comparison of biosurfactants as marine oil spill dispersants: governing factors, synergetic effects and fates, J. Hazard Mater. 416 (2021) 126122.

[6] L. Lisuzzo, et al., Pickering emulsions stabilized by halloysite nanotubes: from general aspects to technological applications, Adv. Mater. Interfac. 9 (10) (2022) 2102346.

[7] R.K. Deshmukh, L. Kumar, K.K. Gaikwad, Halloysite nanotubes for food packaging application: a review, Appl. Clay Sci. 234 (2023) 106856.

[8] M. Massaro, R. Noto, S. Riela, Halloysite nanotubes: smart nanomaterials in catalysis, Catalysts 12 (2) (2022) 149.

[9] S.U. Pickering, Cxcvi.—emulsions, J. Chem. Soc. Trans. 91 (1907) 2001–2021.

[10] Z. Zhu, et al., Recent advancement in the development of new dispersants as oil spill treating agents, Curr. Opin. Chem. Eng. 36 (2022) 100770.

[11] T. Yu, et al., Investigation of amphiphilic polypeptoid-functionalized halloysite nanotubes as emulsion stabilizer for oil spill remediation, ACS Appl. Mater. Interfaces 11 (31) (2019) 27944–27953.

[12] Z. Hu, et al., Surfactant-enhanced cellulose nanocrystal Pickering emulsions, J. Colloid Interface Sci. 439 (2015) 139–148.

[13] O. Owoseni, et al., Microstructural characteristics of surfactant assembly into a gel-like mesophase for application as an oil spill dispersant, J. Colloid Interface Sci. 524 (2018) 279–288.

[14] J. Dong, et al., Modified montmorillonite clay microparticles for stable oil-in-seawater emulsions, ACS Appl. Mater. Interfaces 6 (14) (2014) 11502–11513.

[15] A. Saha, et al., Oil emulsification using surface-tunable carbon black particles, ACS Appl. Mater. Interfaces 5 (8) (2013) 3094–3100.

[16] B.P. Binks, Particles as surfactants—similarities and differences, Curr. Opin. Colloid Interface Sci. 7 (1–2) (2002) 21–41.

[17] O. Owoseni, et al., Interfacial adsorption and surfactant release characteristics of magnetically functionalized halloysite nanotubes for responsive emulsions, J. Colloid Interface Sci. 463 (2016) 288–298.

[18] K.C. Powell, A. Chauhan, Interfacial tension and surface elasticity of carbon black (CB) covered oil–water interface, Langmuir 30 (41) (2014) 12287–12296.

[19] W. Wei, et al., Enhanced efficiency of antiseptics with sustained release from clay nanotubes, RSC Adv. 4 (1) (2014) 488–494.

[20] E. Nyankson, et al., Surfactant-loaded halloysite clay nanotube dispersants for crude oil spill remediation, Ind. Eng. Chem. Res. 54 (38) (2015) 9328–9341.

[21] E. Abdullayev, Y. Lvov, Halloysite clay nanotubes as a ceramic "skeleton" for functional biopolymer composites with sustained drug release, J. Mater. Chem. B 1 (23) (2013) 2894–2903.

[22] E.G. Bediako, et al., Modified halloysite nanoclay as a vehicle for sustained drug delivery, Heliyon 4 (7) (2018) e00689.

[23] Y.M. Lvov, R.R. Price, Halloysite nanotubules, a novel substrate for the controlled delivery of bioactive molecules. Bio-inorganic Hybrid Nanomaterials: Strategies, Syntheses, Characterization and Applications, 2007, pp. 419–441.

[24] E. Nyankson, et al., Ag2CO3-halloysite nanotubes composite with enhanced removal efficiency for water soluble dyes, Heliyon 5 (6) (2019) e01969.

[25] S. Levis, P. Deasy, Characterisation of halloysite for use as a microtubular drug delivery system, Int. J. Pharm. 243 (1–2) (2002) 125–134.

[26] L. Guimaraes, et al., Structural, electronic, and mechanical properties of single-walled halloysite nanotube models, J. Phys. Chem. C 114 (26) (2010) 11358–11363.

[27] E. Nyankson, D. Rodene, R.B. Gupta, Advancements in crude oil spill remediation research after the Deepwater Horizon oil spill, Water, Air, Soil Pollut. 227 (1) (2016) 1–22.

[28] R. Zhai, et al., Immobilization of enzyme biocatalyst on natural halloysite nanotubes, Catal. Commun. 12 (4) (2010) 259–263.

[29] A.E. Frise, et al., Protein dispersant binding on nanotubes studied by NMR self-diffusion and cryo-TEM techniques, J. Phys. Chem. Lett. 1 (9) (2010) 1414–1419.

[30] C.J. Ward, M. DeWitt, E.W. Davis, Halloysite nanoclay for controlled release applications, in: Nanomaterials for Biomedicine, ACS Publications, 2012, pp. 209–238.

[31] B.P. Binks, J.A. Rodrigues, W.J. Frith, Synergistic interaction in emulsions stabilized by a mixture of silica nanoparticles and cationic surfactant, Langmuir 23 (7) (2007) 3626–3636.

[32] H. Katepalli, V.T. John, A. Bose, The response of carbon black stabilized oil-in-water emulsions to the addition of surfactant solutions, Langmuir 29 (23) (2013) 6790–6797.

[33] G. Pi, et al., Novel and environmentally friendly oil spill dispersant based on the synergy of biopolymer xanthan gum and silica nanoparticles, ACS Sustain. Chem. Eng. 4 (6) (2016) 3095–3102.

[34] A. Panchal, et al., Bacterial proliferation on clay nanotube Pickering emulsions for oil spill bioremediation, Colloids Surf. B Biointerfaces 164 (2018) 27–33.

[35] D. Tan, et al., Chapter 8 - surface modifications of halloysite, in: P. Yuan, A. Thill, F. Bergaya (Eds.), Developments in Clay Science, Elsevier, 2016, pp. 167–201.

[36] Y.K. Adofo, et al., Chicken feather protein dispersant for effective crude oil dispersion in the marine environment, ACS Omega (2023).

[37] O. Owoseni, et al., Release of surfactant cargo from interfacially-active halloysite clay nanotubes for oil spill remediation, Langmuir 30 (45) (2014) 13533–13541.

[38] A.D. Venosa, D.W. King, G.A. Sorial, The baffled flask test for dispersant effectiveness: a round robin evaluation of reproducibility and repeatability, Spill Sci. Technol. Bull. 7 (5–6) (2002) 299–308.

[39] P. Luo, et al., Study on the adsorption of Neutral Red from aqueous solution onto halloysite nanotubes, Water Res. 44 (5) (2010) 1489–1497.

[40] D.J. Kraft, et al., Conditions for equilibrium solid-stabilized emulsions, J. Phys. Chem. B 114 (32) (2010) 10347–10356.

[41] Y. Zhu, M.L. Free, Chapter 1 - introduction to surfactants, in: R. Kohli, K.L. Mittal (Eds.), Surfactants in Precision Cleaning, Elsevier, 2022, pp. 1–53.

[42] D.A. Riehm, et al., Dispersion of oil into water using lecithin-Tween 80 blends: the role of spontaneous emulsification, J. Colloid Interface Sci. 487 (2017) 52–59.

[43] J. Penfold, et al., Adsorption at air–water and oil–water interfaces and self-assembly in aqueous solution of ethoxylated polysorbate nonionic surfactants, Langmuir 31 (10) (2015) 3003–3011.

[44] N. Walia, et al., A low energy approach to develop nanoemulsion by combining pea protein and Tween 80 and its application for vitamin D delivery, Food Hydrocoll. Health 2 (2022) 100078.

[45] C.J. Ward, S. Song, E.W. Davis, Controlled release of tetracycline–HCl from halloysite–polymer composite films, J. Nanosci. Nanotechnol. 10 (10) (2010) 6641–6649.

[46] M.M. Calvino, et al., Hydrogel based on patch halloysite nanotubes: a rheological investigation, J. Mol. Liq. 394 (2024) 123721.

[47] M. Fingas, The Basics of Oil Spill Cleanup, third ed., CRC press, USA, 2012, p. 273.

[48] A.D. Venosa, E.L. Holder, Determining the dispersibility of South Louisiana crude oil by eight oil dispersant products listed on the NCP Product Schedule, Mar. Pollut. Bull. 66 (1–2) (2013) 73–77.